

Advanced GIS for Loss Estimation and Rapid Post-Earthquake Assessment of Building Damage

Thomas D. O'Rourke and Sang-Soo Jeon, Cornell University
and Ronald T. Eguchi and Charles K. Huyck, Image Cat, Inc.

Research Objectives

The objectives of the research are to: 1) develop regressions between building damage and various seismic parameters to improve loss estimation, 2) identify the most reliable seismic parameter for estimating building losses, and 3) develop GIS-based pattern recognition algorithms for the identification of locations with most intense post earthquake building damage. This latter objective is coupled to the goal of improving emergency response as part of the MCEER vision of creating earthquake resilient communities. GIS-based technologies for visualizing damage patterns provide a framework for rapidly screening remote sensing data and dispatching emergency services to the locations of greatest need.

Lifeline Damage

MCEER researchers working on the seismic retrofit and rehabilitation of lifelines (Program 1) and on seismic response and recovery (Program 3) have collaborated on a project organized to apply advanced GIS techniques for the rapid identification of locations with most intense building damage. This collaboration has resulted in the development of regressions between building damage and various seismic parameters, as well as the application of GIS-based recognition algorithms with the potential for screening remote sensing data to identify areas of highest post-earthquake damage intensity.

Using GIS technology, Cornell researchers developed the largest U.S. database ever assembled for spatially distributed transient and permanent ground deformation in conjunction with earthquake damage to water supply lifelines (O'Rourke, et al., 1999). This research has helped to delineate local geotechnical and seismological hazards in the Los Angeles region that are shown by zones of concentrated pipeline damage after the Northridge earthquake. The research has resulted in regressions between repair rates for different types of trunk and distribution pipelines and various seismic parameters. The regressions are statistically reliable and have improved predictive capabilities compared with the default relationships currently used in loss estimation programs. They will be referenced in the next version of HAZUS software that implements the National Loss Estimation Methodology sponsored by FEMA. The regressions and statistical databases are being incorporated in pre-standards for estimating water supply losses developed by the American Lifeline Alliance through ASCE under contract with FEMA.

The research has led to the discovery of a relationship for visualizing damage patterns by linking the two dimensional representation of local damage with the grid size used in GIS to analyze the spatial distribution of data. This concept is illustrated in Figure 1 that shows the relationship developed for visualizing post-earthquake pipeline damage (O'Rourke, et al, 1999).

With GIS, the spatial distribution of damage can be analyzed by dividing any map into squares, or cells, each of which is n by n in plan. A repair rate is defined as the number of repairs divided by the total distance of pipelines in each cell. Contours of equal repair rate, or damage rate can then be drawn using the grid of equi-dimensional, n -sized cells. If the contour interval is chosen as the average repair rate for the entire system or portion of the system covered by the map, then the area in the contours represents the zones of highest (greater than average) earthquake intensity as reflected in pipeline damage.

A hyperbolic relationship was shown to exist between the threshold area coverage (TAC) [in this case, the fraction of the total map area with damage exceeding the overall average repair rate] and the dimensionless grid size, defined as the square root of n^2 , the area of an individual cell, divided by the total map area, A_T . This relationship is illustrated in Figure 1, for which a schematic of the parameters is provided by the inset diaphragm. The relationship was found to be valid over a wide range of different map scales spanning 1200 km² for the entire Los Angeles water distribution system affected by the Northridge earthquake to 1 km² of the San Francisco water distribution system in the Marina affected by the Loma Prieta earthquake (Toprak, et al., 1999)

As explained by O'Rourke, et al. (1999) the hyperbolic relationship can be used for damage pattern recognition, and for computer "zooming" from the largest to smallest scales to identify zones of concentrated disruption. If such a relationship can be shown to be valid for building damage, then remote sensing data acquired to characterize building damage can be evaluated rapidly for the locations of highest loss intensity and thereupon targeted for emergency response.

Building Damage

Inspection records available through the California Office of Emergency Services (OES) were obtained for 62,020 buildings that were investigated after the Northridge earthquake. Of these, 48,702 buildings were associated with one and two-story timber frame structures, principally single and multiple family residences. The inspection records include location and estimate of damage as a percentage of replacement cost. Figure 2 shows the types of timber frame structures included in the database with examples of damage, as presented by the NAHB Research Center (1994). The database did not include specific information about the type of damage to each structure.

The number of one to two story timber frame structures affected by the Northridge earthquake was estimated from tax assessor records supplied through OES. The numbers of structures determined in this way was 278,662. As a check, an alternate number was estimated from 1990 census block data (Wessex, 1996) by evaluating the number of buildings associated with detached and attached single housing units in combination with the buildings needed to accommodate two and three to four housing units. The resulting number was 267,868, which is in excellent agreement with the 278,662 units estimated from tax assessor records.

Two damage parameters, referred to as damage ratio and damage factor, were calculated with the database. Damage ratio is the fraction or % of existing structures with damage equal to or exceeding a particular damage factor. Damage factor is damage expressed as a % of building replacement cost.

Loss Estimation Regressions

A GIS grid composed of 2106 cells was created, and the number of relevant structures within each 0.42 km² cell was calculated and geocoded at the cell center. Figure 3 shows the GIS grid developed with tax assessor records superimposed on the spatial variation of peak ground velocity determined from more than 240 strong motion records geocoded as part of this study. By superimposing a grid in which each cell is characterized by various damage ratios linked with damage factors, linear regressions can be performed to quantify damage vs. seismic excitation for loss estimation purposes.

Figures 4a and b show the linear regression of damage ratio (DR) vs. peak ground velocity (PGV) and Spectrum Intensity (SI) for various damage factors (DF). Most regressions for PGV show excellent fits as indicated by high r^2 , although the “goodness” of fit is relatively low for $DF \geq 70\%$. In contrast, all regressions for SI have high r^2 and excellent characteristics with respect to residuals. The relationships between damage and various seismic parameters were probed in this way to determine which parameters were statistically most significant as damage predictors. The seismic parameters investigated include the measured peak ground acceleration, velocity, and displacement; spectral acceleration and velocity for periods of 0.3 and 1.0 s; Arias Intensity; and SI.

SI is defined as the area under the pseudo-velocity, SV, response spectra curve for a damping ratio, ξ of 20 % between periods, T, of 0.1 and 2.5 s:

$$SI = \int_{0.1}^{2.5} SV(T, \xi) DT \quad (1)$$

SI was first proposed by Housner (1959) as a measure of the maximum stresses that would be induced in elastic structures by ground motion. Katayama, et al. (1988) found that house damage correlated more strongly with SI than with peak acceleration, and recommended that SI calculations be performed for $\xi = 20\%$.

An examination of Figure 4 reveals that DR, DF, and the seismic parameter, SP, are interrelated in a consistent way. Using multiple linear regression techniques, this interrelationship can be expressed as

$$\text{Log DR} = \text{Log K} + \alpha \text{ Log SP} - \beta \text{ Log DF} \quad (2)$$

in which K, α , and β are constants. (2) can be rewritten as

$$DR = K(SP/DF^{\beta/\alpha})^\alpha \quad (3)$$

in which $(SP/DF^{\beta/\alpha})$ is the scaled seismic parameter.

Using (3), the data in Figure 4a and b are replotted in Figures 5a and b as linear regressions that account for DR, DF, and SP. As evinced by high r^2 and excellent characteristics with respect to residuals, the relationships in Figure 5a and b are statistically significant.

Seismic parameters normalized with respect to DF combine the effects of strong motion and damage level in a convenient way that facilitates loss estimation. For example, consider

an area for which the predicted SI is 30 cm/sec. The % of timber structures in that area that would have damage equal to or exceeding 10% of the building replacement cost is calculated as $DR = 0.92(30/10^{1.37})^{1.051}$, or 1.19%. For damage equal to or exceeding 50% replacement cost, $DR = 0.92(30/50^{1.37})^{1.051}$, or 0.11%.

Damage Pattern Recognition

Using the same concepts that were applied to the spatial distribution of pipeline damage, investigations were undertaken to define a relationship between TAC (defined for buildings as the fraction of the total map area with DR exceeding the overall average DR) and the dimensionless grid size. The grid containing tax assessor data was sufficiently refined to evaluate the effects of progressively larger grid sizes by developing grids with cell sizes of n by n , $2n$ by $2n$, $4n$ by $4n$, and $8n$ by $8n$. The data generated for these grids and various DFs are plotted in Figure 6. All relationships are well described by hyperbolic functions, similar to the one for pipeline damage in Figure 1. Because building damage is characterized by DF, it has an additional dimension when compared to the single hyperbolic curve for pipelines. In fact Figure 6 is actually a hyperbolic surface for which the initial slopes and asymptotes vary as a function of DF.

Experience has shown that the ideal TAC for visualization is about 0.33. Figure 6 indicates that the dimensionless grid size to achieve this TAC varies significantly, depending on DF.

Figure 7 illustrates the application of Figure 6 for damage intensity recognition and computer “zooming”. The top map shows the entire San Fernando Valley and adjacent areas. The figure shows a cascade of different computer screens that “zoom” on increasingly smaller areas from top to bottom. Each screen shows as blue dots the actual locations of one to two story timber frame structures with $DF \geq 70\%$ after the Northridge earthquake. The red contour lines indicate areas of highest damage intensity.

The contour lines in the top map were generated by analyzing the data with a GIS grid size chosen for $TAC = 0.33$ from Figure 6. The area outlined in red in the top map was identified for more detailed assessment. The grid size for this assessment was again determined for $TAC = 0.33$ from Figure 6. The map in the center of the figure shows an expanded view of the area outlined above after computer analysis. The zones of highest damage intensity for this new map are surrounded by red contour lines.

A similar procedure was followed for the center map in which an area for more detailed assessment was identified within the blue outline. The map at the bottom of the figure shows an expanded view of this new area in which the areas of greatest damage intensity are again surrounded by red contour lines. Increasing density of contour lines reflects increasing intensity of damage. The scale embodied in the bottom map allows the viewer to discriminate damage patterns on virtually a block-by-block basis.

Because the relationships in Figure 6 are independent of scale, the same algorithm for a specific DF can be used for increasingly smaller portions of the original map to “zoom” on areas of most intense damage. The visualization algorithm allows personnel who are not specifically knowledgeable about structures or trained in pattern recognition to identify the locations of most severe damage for allocation of aid and emergency services. The entire process is easy to computerize, and personnel would be able to outline any part of a map with a “mouse” and click on the area so defined. In each instance of defining a smaller area for evaluation, the average DR is recalculated for the new, smaller-sized map. In this way the

average is calibrated to each new map area.

When the damage pattern recognition algorithms are combined with regional data rapidly acquired by advanced remote sensing technologies, the potential exists for accelerated management of data and quick deployment of life and property saving services. By combining work an advanced GIS with advanced remote sensing, MCEER is developing the enabling technologies for a new generation of emergency response and rapid decision support systems.

Summary

GIS research on visualizing damage patterns in pipeline networks has been extended to buildings. Algorithms developed for pipelines have been modified and validated to chose optimal GIS mesh dimensions and contour intervals for visualizing post-earthquake damage patterns in buildings. This work has been performed by a collaboration with researchers working in Programs 1 and 3 on advanced technologies for loss estimation and real-time decision support systems. Robust and statistically significant regressions have been developed between the fraction of existing timber frame buildings at any damage state and the magnitudes of various seismic parameters. Such work improves loss estimation significantly and also creates advanced technology to visualize post-earthquake damage patterns in buildings for rapid decision support and deployment of emergency services.

References

Housner, G. W. (1959), "Behavior of Structures During Earthquakes", Journal of Engineering Mechanics Division, ASCE, Vol. 85, No. EM4, pp. 109-129

Katayama, T., N. Sato, and K. Saito (1988), "SI-Sensor for the Identification of Destructive Earthquake Ground Motion", Proceedings, 9th World Conference on Earthquake Engineering, Vol. VII, Tokyo-Kyoto, Japan, Aug., pp. 667-672

NAHB Research Center (1994), "Assessment of Damage to Residential Buildings Caused by the Northridge Earthquake", Reported Prepared for U.S. Department of Housing and Urban Development by NAHB Research Center, Upper Marlboro, MD

O'Rourke, Thomas D., Selcuk Toprak, and Sang-Soo Jeon (1999), "GIS Characterization of the Los Angeles Water Supply, Earthquake Effects, and Pipeline Damage", Research Progress and Accomplishments 1997-1999, Multidisciplinary Center for Earthquake Engineering Research, University at Buffalo, State University of New York, Buffalo, New York, July, 1999, pp. 45-54.

Toprak, S., T.D. O'Rourke, and I. Tutuncu (1999), "GIS Characterization of Spatially Distributed Lifeline Damage", Proceedings, 5th US Conference on Lifeline Earthquake Engineering, Seattle, WA, Aug., in press.

Wessex (1996), "U.S. Demographics", Wessex, Inc., Winnetka, IL

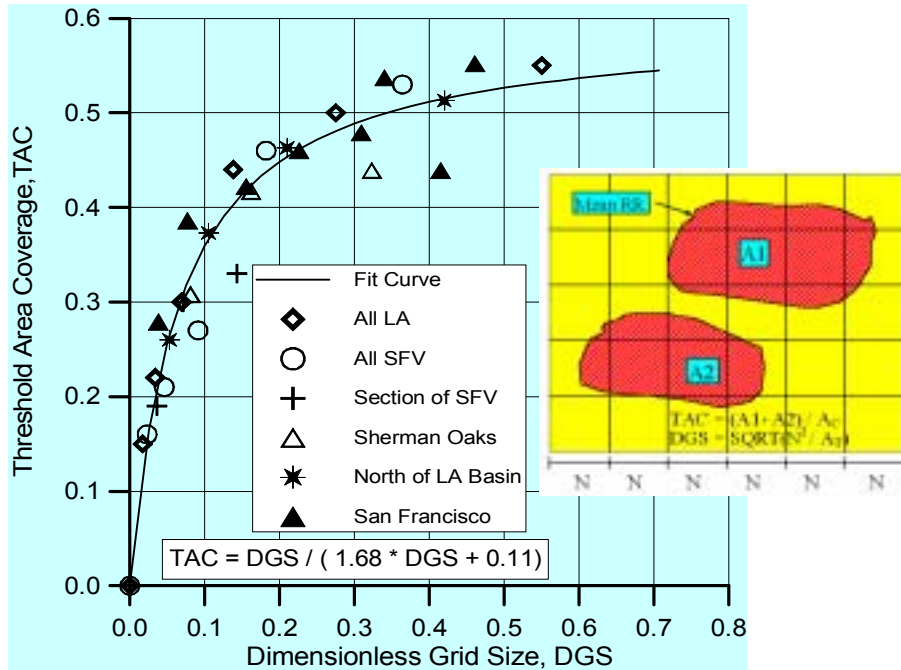


Figure 1. Hyperbolic Fit for Threshold Area Coverage and Dimensionless Grid Size for Pipeline Damage Patterns (Toprak, et al., 1999)



a) Foundation Cripple Wall Collapse



b) Racking of Walls

c) Roof Framing Damage

Figure 2. Typical Damage to 1-2 Story Timber Frame Buildings after the Northridge Earthquake (after NAHB, 1994)

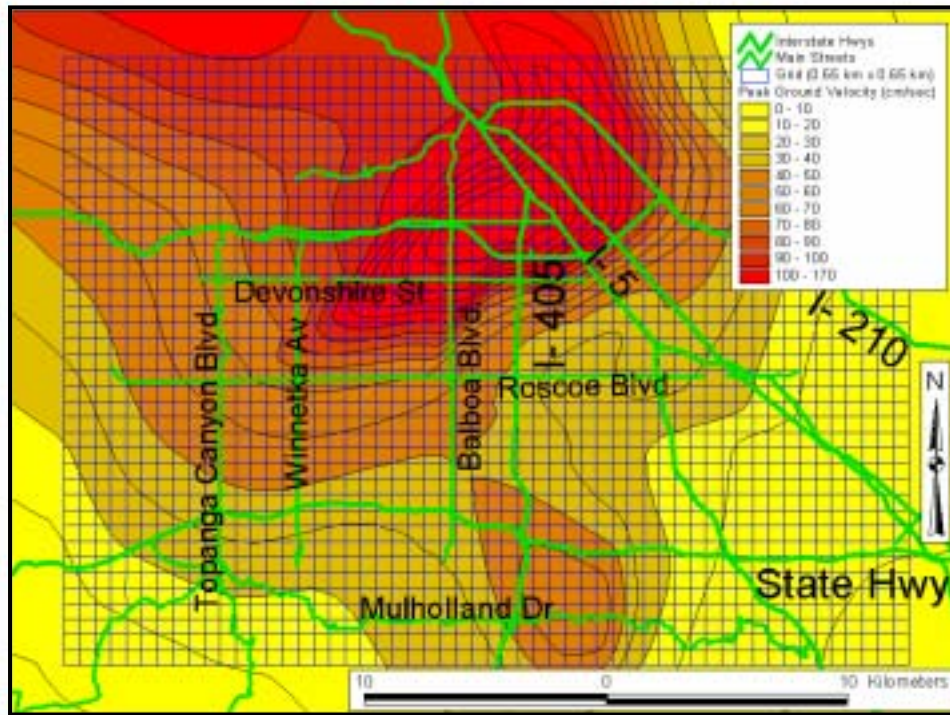


Figure 3. GIS Grid with Tax Assessor Data Superimposed on Peak Ground Velocities

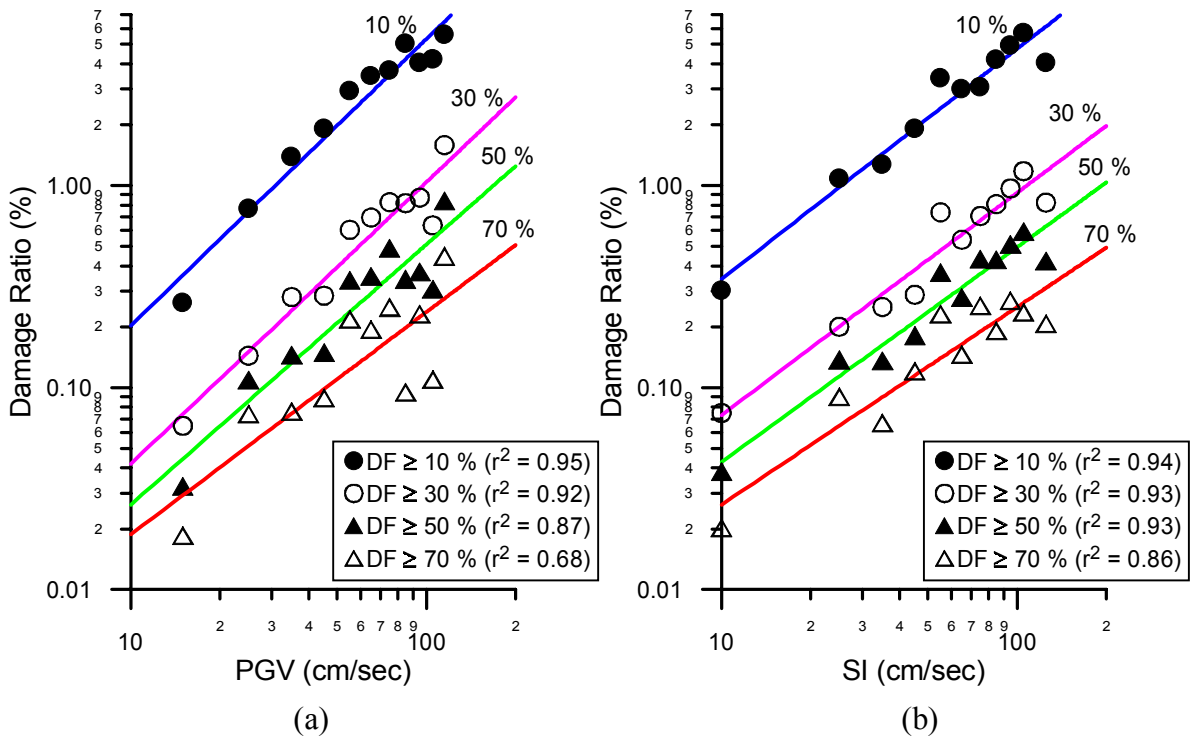


Figure 4. Damage Ratio Regression with Peak Ground Velocity (PGV) and Spectrum Intensity (SI) for 1-2 Story Timber Frame Buildings

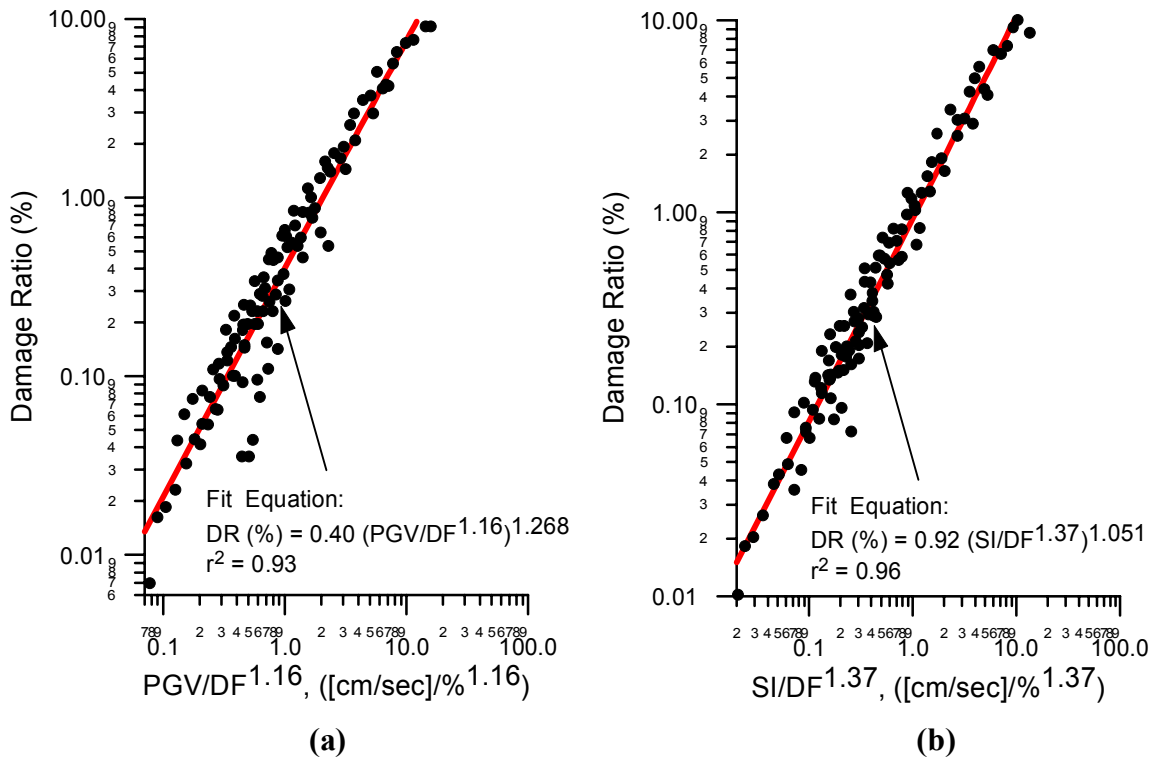


Figure 5. Damage Ratio Regression for Scaled PGV and SI for 1-2 Story Timber Frame Buildings

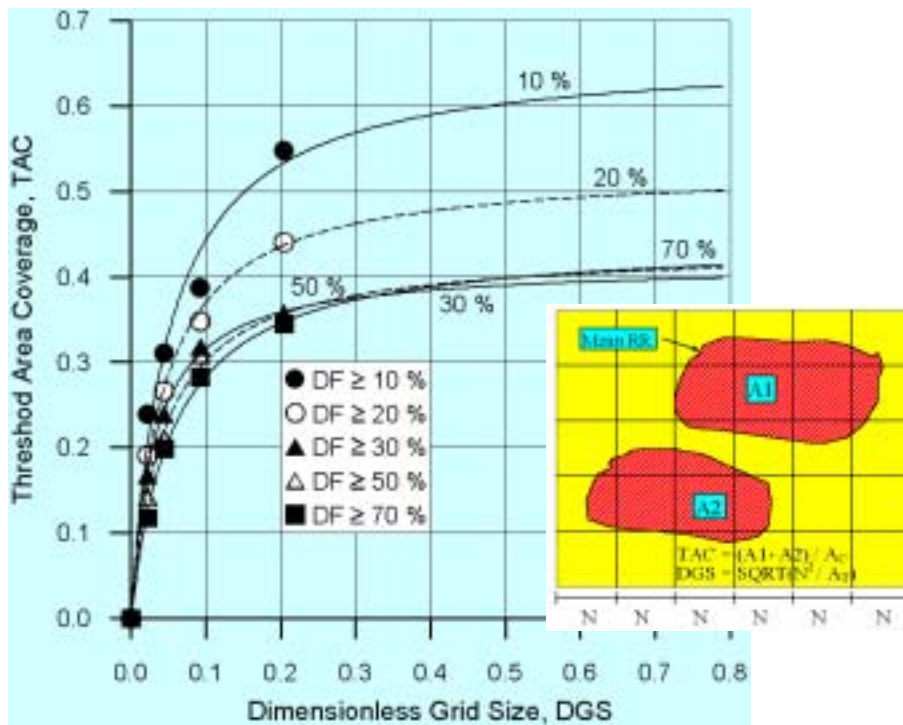


Figure 6. Hyperbolic Fit for Threshold Area Coverage and Dimensionless Grid Size for 1-2 Story Timber Frame Buildings

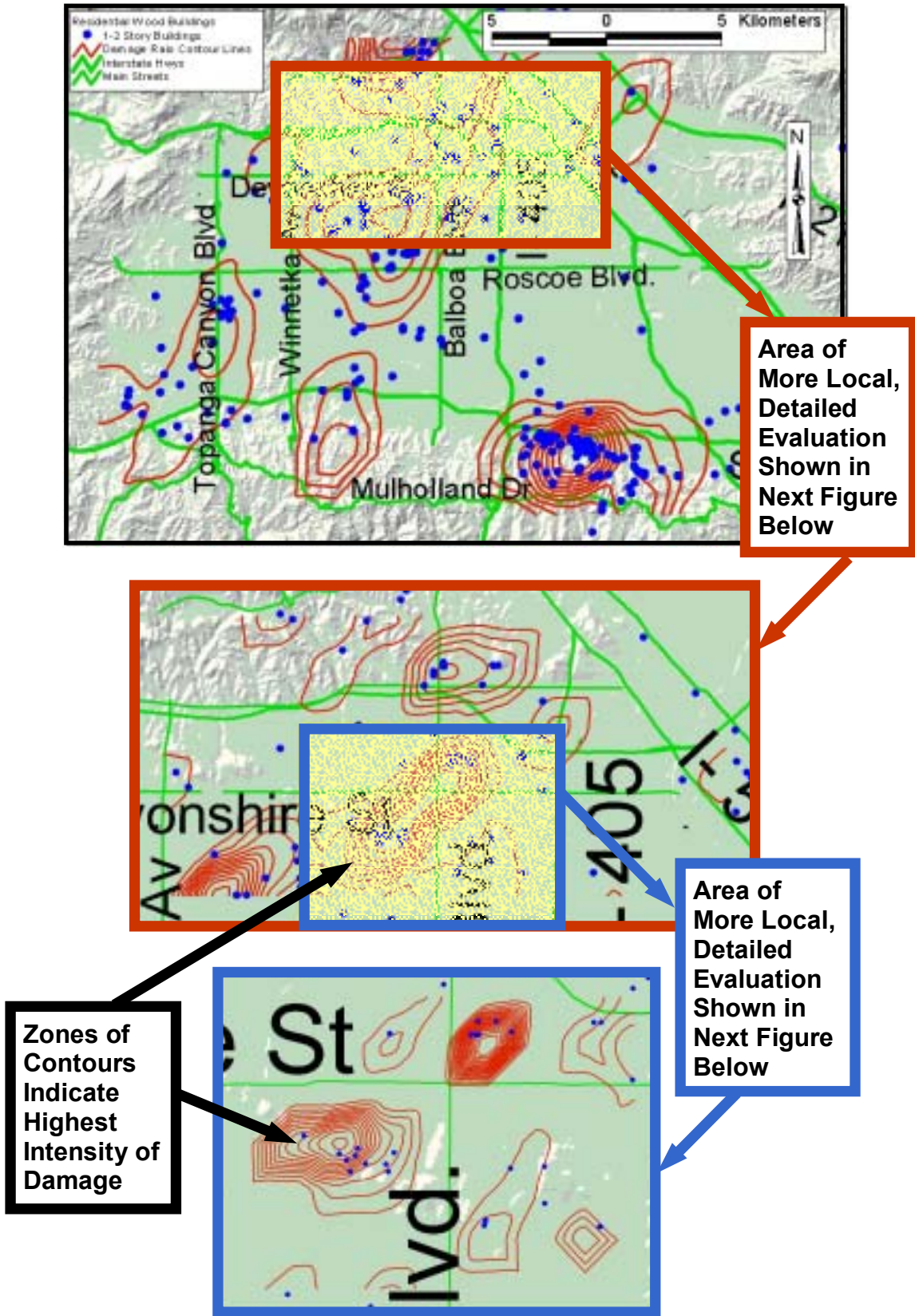


Figure 7. GIS Evaluation of Building Damage for DF ≥ 70 %